



Nanomechanical three dimensional force photonic crystal sensor using shoulder-coupled resonant cavity with an inserted pillar



Yi Yang^a, Huiping Tian^{a,b}, Daquan Yang^{a,c}, Nannan Wu^a, Jian Zhou^a, Qi Liu^a, Yuefeng Ji^{a,*}

^a State Key Laboratory of Information Photonics and Optical Communications, School of Information and Communication Engineering, Beijing University of Posts and Telecommunications, Beijing 100876, China

^b Key Laboratory of Micro and Nano Photonic Structures (Ministry of Education), and State Key Laboratory of Surface Physics, Fudan University, Shanghai 200433, China

^c School of Engineering and Applied Sciences, Harvard University, Cambridge, MA 02138, USA

ARTICLE INFO

Article history:

Received 7 October 2013
Received in revised form 7 January 2014
Accepted 9 January 2014
Available online 18 January 2014

Keywords:

Optical sensing and sensors
Photonic crystals
Optical resonators
Multi-dimensional force sensor

ABSTRACT

A nanomechanical three-dimensional force photonic crystal (PhC) sensor is proposed in this paper by using a shoulder-coupled aslant resonant nanocavity with a single inserted Si pillar and the sensing characteristics are theoretically analyzed and demonstrated. This sensor can be used to detect nanomechanical force in three orthogonal directions independently by measuring the shift of resonant wavelength. The aslant resonant cavity with high quality factor of 7800 ensures high force sensing sensitivity in every dimension as the sensitivity can be enhanced by optimizing the cavity. The shoulder-coupled PhC structure and mobile Si pillar ensure the sensor can detect force from every direction. By applying finite element method (FEM) and finite difference time domain (FDTD) simulations, sensing sensitivity of 8.2, 12.5 and 10.9 nm/ μN have been achieved in three dimensions and limitation of the smallest detectable force is 24, 16 and 18 nN in three dimensions, respectively.

© 2014 Elsevier B.V. All rights reserved.

1. Introduction

A nanomechanical sensor is the device to detect nanomechanical variations such as deformation, force, acceleration, displacement and so on. It has been broadly used in microelectromechanical system (MEMS) as sensing is the key part in the whole process when forming MEMS. Most of the nanomechanical sensors researched in recent decades were based on fibers [1–3] or carbide [4,5]. However, a huge obstacle is impassable when integrating fibers, carbide with common silicon devices. Sensors utilizing photonic crystal (PhC) based on silicon can easily solve this problem because their convenience to be integrated with silicon devices and small scale size.

PhC has been attracting an increasing interest since Yablonovitch and John proposed in 1987, respectively [6,7]. In the past few years, different kinds of PhC sensors used in biosensing [8–10], gas sensing [11,12] and temperature sensing [13] have been come up. Optical nanomechanical sensors [14–19] based on PhC have been also researched for its ultra-small size, high sensitivity and ease of integration with Si devices. For example, Lee

et al. presented the design and optimization of a nanomechanical sensor by using U-shaped silicon PC waveguide to detect micro-strain [14], Yang et al. demonstrated a novel nanoscale photonic crystal pressure sensor with PhC waveguides and piston-type microcavity [15], Li et al. investigated a nano-scale force and pressure sensor by integrated with three nano-ring resonators together [16], Tian et al. demonstrated the relationship between out-of-plane nanomechanical deformations and the tuning of double-coupled one-dimensional photonic crystal cavities [17], Winger et al. presented a nanocavity with electromechanical and optomechanical characteristics, which combined with an electrical circuit with a high quality factor PhC nanocavity to realize electrokinetic sensor [18] and Yang et al. proposed a method to detect nano-stress in two dimensions within a single PhC structure [19]. Most of the nanomechanical sensors mentioned above provide ultra high sensitivity [14,19] and they are very small in size [15,16] so that they can be used in MEMS. However, the sensors can only detect nanomechanical variation in one dimension, and they are difficult to be integrated to realize sensing of the nanomechanical variation in three dimensions. The ability to sense nanomechanical variation in more than one dimension is requisite and it would be best for designing a single structure to realize this function.

In this paper, we propose a three dimensional photonic crystal nanomechanical sensor based on shoulder-coupled resonant nanocavity with an inserted pillar which can be used to detect the nanomechanical variation in three dimensions with high

* Corresponding author at: P.O. Box 90, BUPT, No. 10, Xitucheng Road, Haidian District, Beijing 100876, China.

E-mail addresses: iceman-966@163.com (Y. Yang), hptian@bupt.edu.cn (H. Tian), jyf@bupt.edu.cn (Y. Ji).

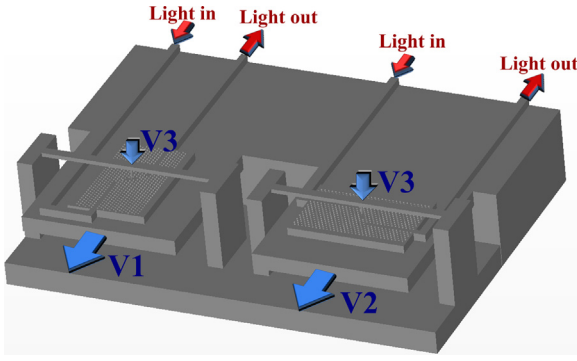


Fig. 1. Schematic of the nanomechanical three dimensional force sensor design. Force is applied in horizontal direction (V1), vertical direction (V2) and upright direction (V3), respectively.

sensitivity and the characteristics of the sensor are theoretically analyzed. The structure is formed by a pillar-inserted aslant nanocavity which is shoulder-coupled by two W1 waveguides. Light is injected into the aslant cavity through the input waveguide and the light leaked from the cavity is monitored at the end of the output waveguide. A sharp peak corresponding to the resonant wavelength in the transmittance spectra is used as pointer to detect the nanomechanical variation. As shown in Fig. 1, when the nanomechanical force is applied on the structure from one direction in the plane, the mechanical deformation of the PhC structure caused by the force will shift the resonant wavelength. When the nanomechanical force is applied from the direction perpendicular to the plane, the pillar will be inserted into the tiny air hole in the middle of the cavity and the resonant wavelength will be also shifted because the variation of the cavity affects the resonant wavelength. The value of force can be known through the displacement of the resonant wavelength shift because of the linear relationship between the displacement of shift and the applied mechanical force. In this paper, firstly we will introduce the theory of nanomechanical variation sensing and the design of PhC structure. The optical properties of the cavity and the whole structure will be investigated by the finite difference time domain (FDTD) simulations. Then the mechanical variations caused by force in three dimensions will be investigated by the finite element method (FEM) simulations, respectively. Finally by combining the results of FDTD and FEM simulations together we will discuss the sensing properties of the structure in the every direction, respectively.

2. Theoretical analysis and design principle

2.1. Nanomechanical force sensing principle

When the nanomechanical force is applied on the optical force sensor, the deformations of the sensing structure caused by the force will lead to some variation of the optical properties. And there are two ways to detect the value of force by measuring the variation of transmitted intensity [15,20] or the shift of specific wavelength [16,19,21–23]. We choose to measure the shift of resonant wavelength in our study because the intensity of resonant wavelength varies a little under different value of force in our study and this will arouse inaccuracy in the measurement of nano-force. As shown in Fig. 1, the force from horizontal direction (V1), vertical direction (V2) parallel to the PhC slab plane and upright direction (V3) perpendicular to the PhC slab plane will all cause the variation of the resonant cavity, and the resonant wavelength of the cavity will shift, respectively. By applying FEM and FDTD simulations we can calculate the value of force by measuring the displacement of resonant wavelength.

2.1.1. Force parallel to slab plane

V1 and V2 in Fig. 1 show the nano-force (F) is applied parallel to the plane in two directions and Fig. 2(a) and (b) shows the schematic deformation of the air holes under force of V1 and V2. The point force is applied on the edge of the substrate so that the PhC structure fixed on the substrate can generate geometric variation. The air holes' geometries and positions on the PhC slab are all modified and the resonant wavelength will shift due to the corresponding variation of PhC structure. With FDTD simulations, the shift of resonant wavelength ($\Delta\lambda$) can be obtained. Here, we define the sensitivity (S_a , nm/ μN) of this nanomechanical force sensing structure when force is applied parallel to the plane in horizontal or vertical direction as follow:

$$S_a = \frac{\Delta\lambda}{\Delta F} \quad (1)$$

where $\Delta\lambda/\Delta F$ represents the displacement of resonant wavelength caused by the applied force. In addition, the limit of nano-force detection L_a (nN) when force is applied parallel to the slab plane can be defined as the minimum detectable force variation, however, the force variation is reflected by the shift in the transmission spectrum, that is the minimum spectral resolution of measured light wave, which is decided by the measured optical line-width in spectrum, or equivalently, Q factor. Therefore with the substitution of Eq. (1), L_a is defined as follow:

$$L_a = \frac{\Delta F}{\Delta\lambda} \times \frac{\lambda_c}{Q} = \frac{\lambda_c}{S_a Q} \quad (2)$$

where, λ_c , Q , and λ_c/Q represent the resonant wavelength, the quality factor of the cavity, and the line-width of the transmission peak, respectively. From Eq. (2), we know that the detectable limit L_a is mainly affected Q . And smaller L_a can be achieved with higher quality factor when the force is applied in horizontal direction and vertical direction in Fig. 1 parallel to the slab plane.

2.1.2. Force perpendicular to the slab plane

V3 in Fig. 1 shows the force perpendicular to the slab plane is applied on the structure and the single pillar is inserted into the air hole in the middle of the cavity under force in upright direction as shown in Fig. 2(c). The point force in V3 direction is applied on the center of the Si strip. Similarity to the force applied parallel to the plane, we can get the sensitivity S_d (nm/ μN) of this nanomechanical force sensor when force is applied perpendicular to the plane in upright direction, but firstly the sensitivity S_b (nm/ μN) between the corresponding depth of the pillar inserted into the tiny air hole Δh (nm) and the applied force applied perpendicular to the slab plane should be studied. Here, we define S_b as follow:

$$S_b = \frac{\Delta h}{\Delta F} \quad (3)$$

where $\Delta h/\Delta F$ represents the inserted depth of the pillar caused by specific applied force. Secondly, we define the sensitivity S_c (nm/ μN) between the inserted depth (Δh) and the corresponding displacement of resonant wavelength ($\Delta\lambda$) as follow:

$$S_c = \frac{\Delta\lambda}{\Delta h} \quad (4)$$

where $\Delta\lambda/\Delta h$ represents the shift of the resonant wavelength caused by the inserted depth of the pillar. Finally, combining with Eq. (3) and Eq. (4), the sensitivity in upright direction S_d can be achieved as follow:

$$S_d = S_b \times S_c = \frac{\Delta h}{\Delta F} \times \frac{\Delta\lambda}{\Delta h} = \frac{\Delta\lambda}{\Delta F} \quad (5)$$

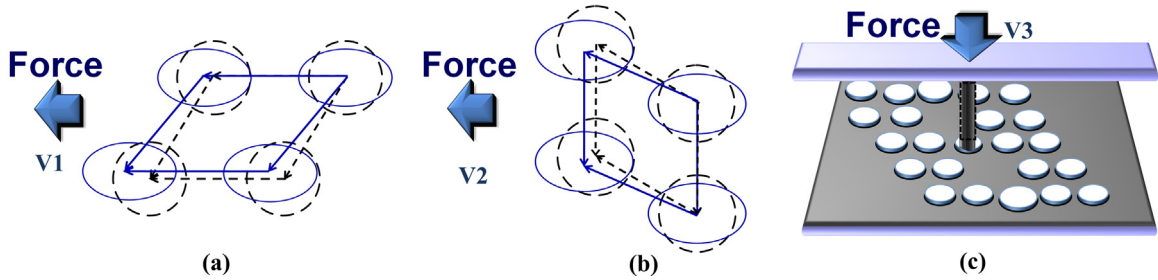


Fig. 2. Schematic of air holes' variations when force is applied in V1 direction (a) and V2 direction (b). Variation of the Si strip and the Si pillar when force is applied in V3 direction (c).

With Eq. (5), the limit of nano-force detection L_b (nN) when force is applied perpendicular to the slab plane can be defined the same as L_a :

$$L_b = \frac{\Delta F}{\Delta h} \times \frac{\Delta h}{\Delta \lambda} \times \frac{\lambda_c}{Q} = \frac{\lambda_c}{S_d Q} \quad (6)$$

where λ_c , Q and λ_c/Q represent the resonant wavelength and the quality factor of the cavity, respectively. The same as L_a , smaller L_b can be obtained with higher quality factor of the resonant cavity.

2.2. Sensor structure design

The whole sensor structure based on a shoulder-coupled aslant nanocavity with a tiny air hole and a single Si pillar is presented in Fig. 3(a). A silicon pillar is bonded on a Si strip which is just above the tiny air hole in the middle of aslant cavity and completely out of the tiny air hole when the force is free as shown in Fig. 3(b). And the Si PhC slab structure, which is the key part of the nanomechanical force sensor, is clearly shown in Fig. 3(c) and (d). The Si slab PhC structure is formed by triangular lattice air holes and the refractive index of silicon is $n_{Si} = 3.48$. The PhC structure consists of an optimized aslant cavity and two coupling W1 waveguides. We set the lattice constant is $a = 417$ nm, the radius of bulk air holes is $r = 0.3a = 125.1$ nm and the thickness of the PhC slab is $t_1 = 0.56a = 233.5$ nm. Then we set the thickness of the Si strip is $t_2 = 226$ nm, width is $w = 5 \mu\text{m}$, and length is $l = 30 \mu\text{m}$. The radius of the Si pillar is $r_p = 0.21a = 87.5$ nm. In our research, we use open source 3D FDTD simulation software Meep [24] to study the confinement of the aslant cavity and achieve the transmittance spectra. In our FDTD simulation analysis, a mesh size of $a/20$ and time step of $0.025a/c$ are employed, where a is the lattice constant. All the simulations are carried out with the same mesh size and time step for future comparable results. Since the boundary conditions at the spatial edges of the computational domain must be carefully considered. The simulation area in our paper is surrounded by one-spatial unit thick perfectly matched layer (PML), in which both electric and magnetic conductivities are introduced in such a way that the wave impedance remains constant, absorbing the energy without inducing reflections.

The shoulder-coupled aslant nanocavity with an inserted pillar is formed firstly by removing three air holes along the oblique direction in the center area as shown in Fig. 3(c) and the two air holes close to the point defects along the oblique line are shifted outwards. Secondly, we adjust the outward shift of the two outer holes s . Thirdly, we adjust the radius of the two outer holes r_o to achieve higher quality factor and stronger confinement of the aslant cavity. Finally, we add one tiny air hole in the center of the cavity and adjust the radius r_c of the center air hole to obtain higher quality factor for higher sensitivity as Eq. (1) and Eq. (5) indicated.

We used 3D FDTD software to design and optimize the aslant cavity by adjust these parameters mentioned before. We take consideration on two key optical characteristics: quality factor and resonant frequency of the cavity. Firstly we obtain the variation tendency of quality factor and resonant frequency of the cavity without a tiny air hole in the center for simplicity by increasing the shift s from $0.1a$ to $0.3a$ with an increment of $0.01a$ and the radius of the two outer holes are constant as others'. Fig. 4(a) presents the variation tendency of the resonance frequency and quality factor with the change of the shift. From Fig. 4(a) we observe the resonant frequency decreases from $0.2561(2\pi c/a)$ to $0.2428(2\pi c/a)$ when the hole shift increases due to the larger shift will bring in more high-dielectric material in the region of cavity, but the highest quality factor is obtained when $s = 0.2a$ and the peak value is 3500. Secondly, when the shift of outer holes is $s = 0.2a$, we obtain the variation tendency of quality factor and resonant frequency of the cavity without a tiny air hole in the center by increasing r_o from $0.3a$ to $0.5a$ with an increment of $0.01a$. From Fig. 4(b) we observe the resonant frequency increases from $0.2484(2\pi c/a)$ to $0.2695(2\pi c/a)$ when r_o increases as bigger air holes will decrease the high-dielectric material in the region of cavity, the highest quality factor is obtained when $r_o = 0.39a$ and the peak value is 4900. Thirdly, when $s = 0.2a$ and $r_o = 0.39a$, we add a tiny air hole in the center of the aslant cavity and we obtain the variation tendency of quality factor and resonant frequency of the cavity by increasing the radius of the added air hole r_c from $0a$ to $0.3a$ with an increment of $0.01a$. From Fig. 4(c) we observe the resonant frequency increases from $0.2611(2\pi c/a)$ to $0.2718(2\pi c/a)$ when r_c increases due to the decrease in high-dielectric material in the cavity region, the highest quality factor is obtained when $r_c = 0.21a$ and the peak value is 7800.

When the parameters of s , r_o and r_c are set to be $0.2a$, $0.39a$ and $0.21a$, respectively, we consider the relationship between the depth of the Si pillar inserted into the center tiny air hole and the optical characteristics of the aslant cavity. Fig. 4(d) presents the variation tendency of the resonance frequency and quality factor with the change of Δh . We simulate the situations by increasing Δh from $0a$ to $0.55a$ with an increment of $0.05a$. From Fig. 4(d), we observe the resonant frequency decreases from $0.2671(2\pi c/a)$ to $0.2577(2\pi c/a)$ when the depth Δh increases because the inserted pillar introduce more high-dielectric material into the cavity. However, the quality factor does not vary a lot and stay relatively stable when Δh changes. This is because when the force from upright direction is applied on the Si strip, the variation of the Si strip makes the pillar inserted in the center tiny hole and so there is little influence on the slab PhC structure. Therefore, the quality factor keeps steady when Δh changes and this cavity with a pillar allows us to detect the small variation in the upright direction perpendicular to the slab plane.

When the parameters of $s = 0.2a$, $r_o = 0.39a$, $r_c = 0.21a$ and $\Delta h = 0a$ are set, in order to demonstrate the ability of the cavity in

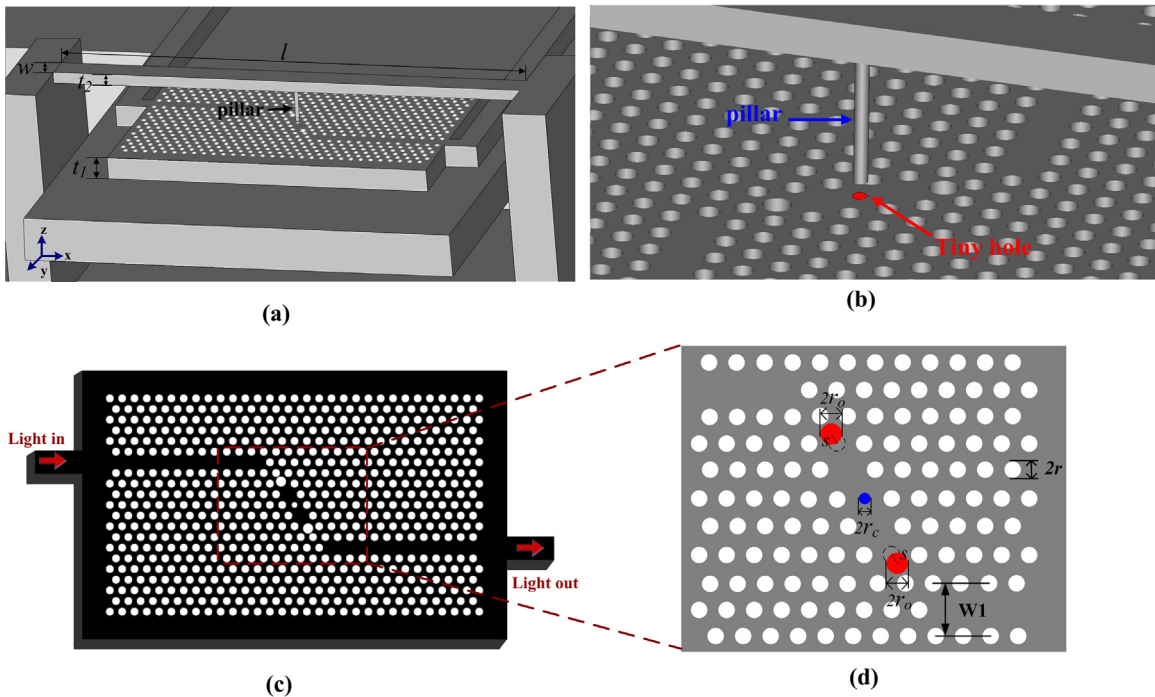


Fig. 3. (a) Schematic of the sensor design, where $t_1 = 233.5$ nm, $t_2 = 226$ nm, $w = 5$ μm and $l = 30$ μm . (b) Detail of the Si pillar and the slant cavity area. (c) The top view of simulated PhC structure. (d) Zoom in the slant cavity area and the detail of the air holes, where $a = 417$ nm, $r = 0.3a$, $s = 0.2a$, $r_o = 0.39a$, $r_c = 0.21a$ and $w_1 = \sqrt{3}a$.

confining light, we put a narrow band TE-like polarization light source in the middle of the cavity and simulate the electric field distribution in the cavity. From Fig. 5(a), we can see the dark blue and red area located in the cavity which means the cavity has strong

ability to confine light. In order to inject and light in the slant cavity and get the transmittance spectra, the slant cavity with a pillar is shoulder-coupled by one W1 input waveguide and one W1 output waveguide as shown in Fig. 3(c). Then we put a TE-like

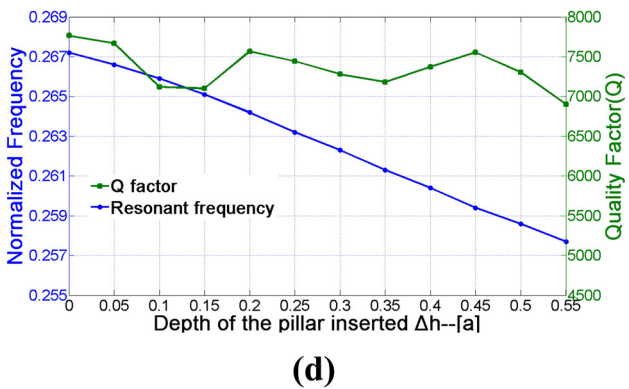
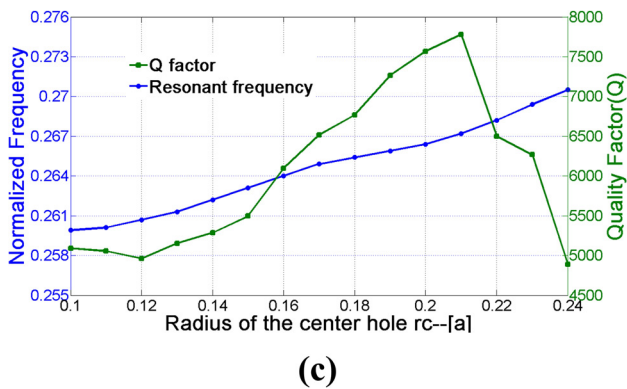
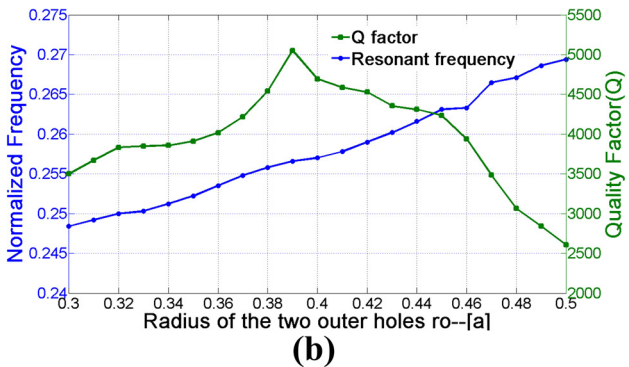
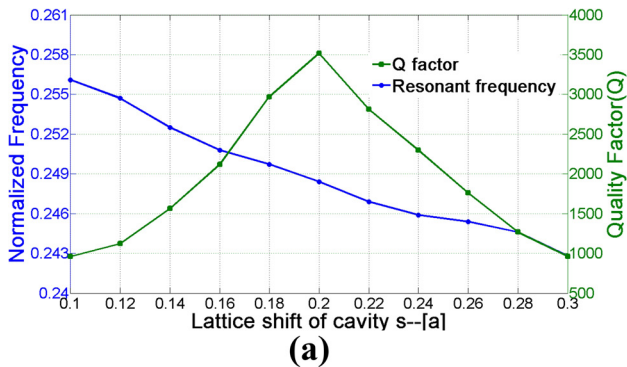


Fig. 4. (a) The variation trend of the cavity's resonant frequency and quality factor with the change of s , the lattice shift along the oblique direction. (b) The variation trend of the cavity's resonant frequency and quality factor with the change of r_o , the radius of the two outer air holes. (c) The variation trend of the cavity's resonant frequency and quality factor with the change of r_c , the radius of the tiny center air hole. (d) The variation trend of the cavity's resonant frequency and quality factor with the change of Δh , inserted depth of the Si pillar.

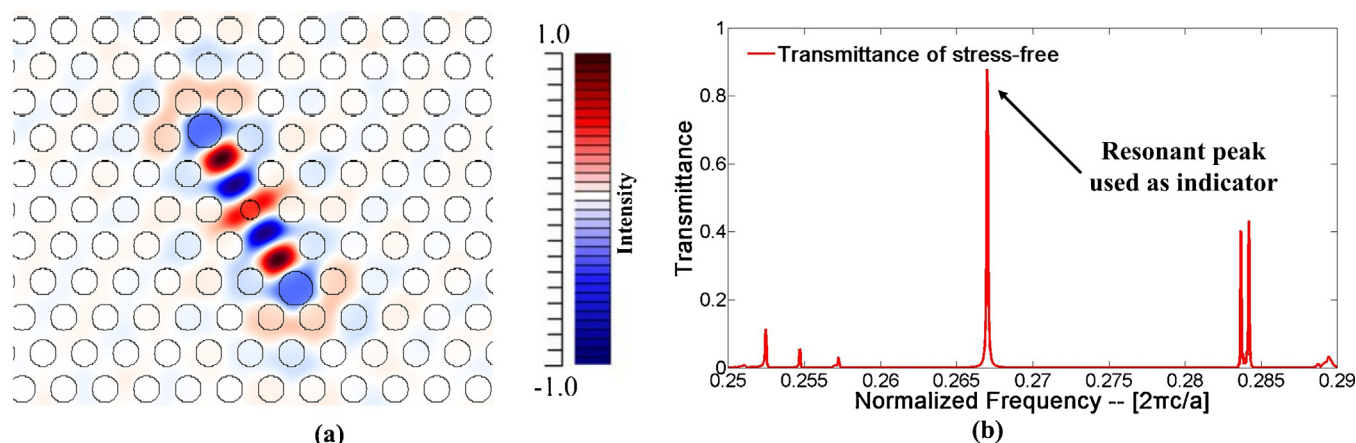


Fig. 5. (a) Electric field distribution in x - y plane of the slant cavity by using 3D FDTD simulations. (b) Transmittance spectra of original PhC structure without force loaded.

polarization Gaussian-pulse light source before the input waveguide, from the end of output waveguide transmittance spectra can be got. The transmittance spectra of force-free PhC structure are shown in Fig. 5(b). From Fig. 5(b), we can see the resonant peak appears at $0.2670(2\pi c/a)$ and the corresponding resonant wavelength λ_c is 1561.8 nm. In our study, we use this resonant peak as indicator to detect the nanomechanical force when force is applied in every direction because the cavity is carefully optimized and the quality factor is quite high to achieve high sensing sensitivity. In the future fabrication process of sensor, this kind of Si PhC structure and the pillar inside a nanometer size air hole can be realized with EBL (e-beam lithography) technique and deep reactive ion etching[25,26].

3. Variations of the structure under nanomechanical force

In order to investigate the mechanical characters of the PhC structure and the single pillar, commercial software ANSYSTM 13.0 was used to investigate the nanomechanical variation under applied force in three directions. With the FEM software, we construct a 3D solid model the same as shown in Fig. 3 to simulate the nanomechanical deformations under various force. Physical parameters of Si are set as follow: density is for 2330 kg/m^3 , Young's modulus is 169 GPa and Poisson's ratio is 0.28. The size of the Si PhC slab structure is set as follow: thickness (t_1) is 233.5 nm, width is $15 \mu\text{m}$ and length is $15 \mu\text{m}$. The material of the model is set to be linear, elastic and isotropic. We simulated the structural variation when nanomechanical force was applied in V1 and V2 in Fig. 1, where the force (F , in micro Newton unit) considered were 0.2, 0.4, 0.6, 0.8 and $1 \mu\text{N}$. Both horizontal direction and vertical direction were loaded respectively to see the variations of air holes. Fig. 6(a) and (b) shows the deformed PhC slab structure contour plot of displacement vector sum in the x - y plane with the applied force of $1 \mu\text{N}$ in the two directions, respectively.

The pillar is fixed on the Si strip so that the pillar will be inserted into the center tiny air hole when force is applied on the middle of the Si strip in upright direction as shown in Fig. 7(a). The displacement in the middle of the Si strip is the same as the inserted depth of the pillar (Δh). Therefore, we can study the variation of the Si strip to know the variation of Δh . We set thickness, width, and length of the Si strip to be $t_2 = 226 \text{ nm}$, $w = 5 \mu\text{m}$, and $l = 30 \mu\text{m}$, respectively. With FEM simulations, Fig. 7(b) shows the simulation result of deformation in upright direction when $1 \mu\text{N}$ is applied on the middle of the Si strip. The variation of inserted depth (Δh) has been studied when applied force on the Si strip (F) varies from 0 to $1 \mu\text{N}$. As seen in Fig. 7(b), the inserted depth (Δh) varies

linearly when the applied force F is changing in the range of our study.

4. Characteristics discussion combining with FEM and FDTD simulations

With the FEM software we have achieved the deformations of the PhC structure and the Si pillar under various applied force in different directions, then all the deformations are modeled and simulated by the 3D FDTD software to achieve the transmittance spectra. In Section 2.1.1, we have explained the principle to detect the value of force by measuring the shift of resonant wavelength. In this section, we will discuss the sensing properties in every dimension, respectively.

4.1. Force applied parallel to slab plane

When the force is applied in V1, we can see the simulation results show shift of the resonant wavelength and the peaks are evenly distributed when the force varies from 0 to $1.00 \mu\text{N}$ in Fig. 8(a). The resonant wavelength shifts towards shorter wavelength (blue-shift) when the force is applied in horizontal direction. As shown in Fig. 8(b), similarly when the force is applied in V2 varying from 0 to $1.00 \mu\text{N}$, the resonant wavelength shifts towards longer wavelength (red-shift) and the peaks are evenly distributed as well.

Combining with FEM and 3D FDTD simulation results together, the force sensing sensitivity S_a of 8.2 and $12.5 \text{ nm}/\mu\text{N}$ in the horizontal and vertical direction, respectively, has calculated according to Eq. (1). Hence, by plugging λ_c , Q and S_a into Eq. (2), the detectable limit L_a of 24 and 16 nN can be achieved in the horizontal and vertical direction, respectively.

4.2. Force applied perpendicular to slab plane

Similarity to the force applied parallel to the slab plane, when the force is applied in V3, we can see the resonant wavelength shifts towards longer wavelength (red-shift) and the peaks are evenly distributed when the force varies from 0 to $1.00 \mu\text{N}$ in Fig. 9. Force sensing sensitivity S_d in upright direction can be calculated to be $10.9 \text{ nm}/\mu\text{N}$ according to Eq. (5). Furthermore, by plugging λ_c , Q and S_d into Eq. (6), the detectable limit L_b of 18 nN is obtained in upright direction.

The relationship between the applied nanomechanical force F in three directions and the corresponding displacement of resonant wavelength $\Delta\lambda$ has been shown in Fig. 10 with the simulation results in Figs. 8(a and b) and 9. In Fig. 10, we can see that the

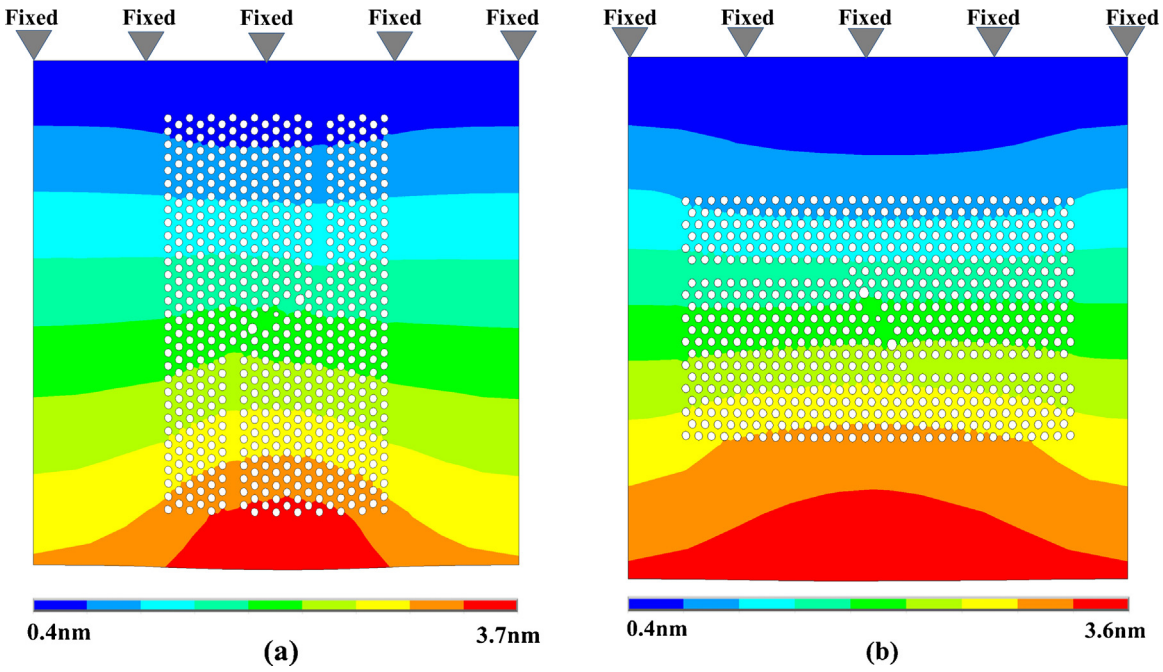


Fig. 6. Deformation contour plot of the PhC structure in x - y plane under $1 \mu\text{N}$ force load in V1 direction (a) and V2 direction (b) simulated by FEM software as viewed from the top.

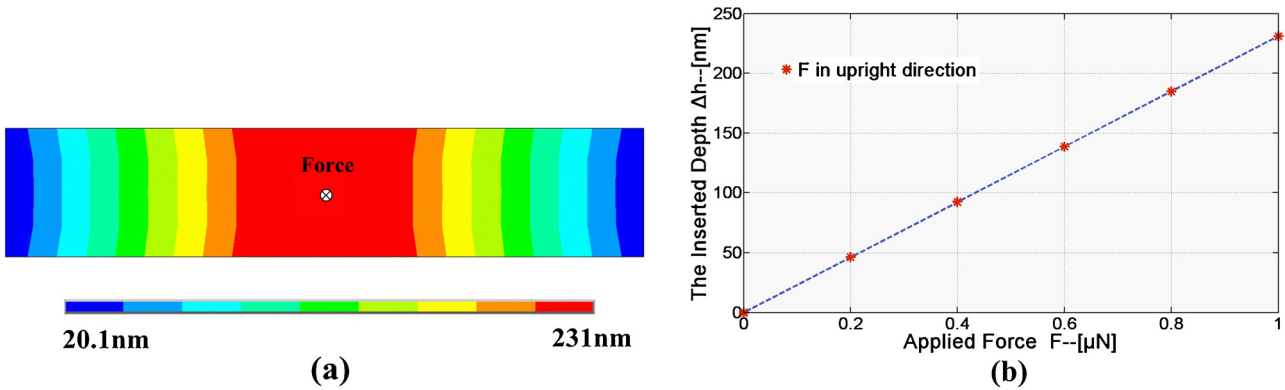


Fig. 7. (a) Displacement in z -direction of the Si strip under $1 \mu\text{N}$ force load in V3 direction viewed from the top. (b) The structural variation (Δh) as the function of the applied force F in V3 direction.

relationship between F and $\Delta\lambda$ in all directions are linear in the range of our study. From the discussion above, we know that the nanomechanical force sensing sensitivity in three directions are very high in the same level and the detection limit are ultra small

which means this shoulder-coupled aslant resonant nanocavity with an inserted pillar design is a practicable method to detect nanomechanical force applied both parallel and perpendicular to slab plane in three dimensional space.

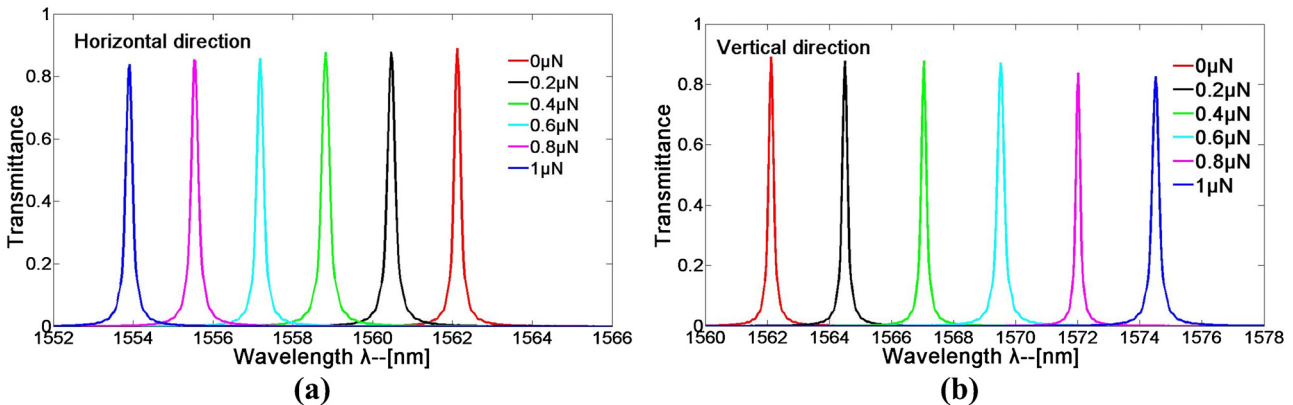


Fig. 8. Transmittance spectra showing the shift of resonant wavelength under different force in V1 direction (a) and V2 direction (b).

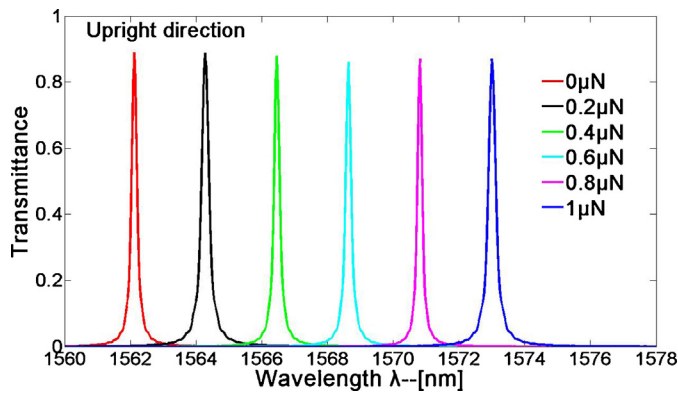


Fig. 9. Transmittance spectra showing the shift of resonant wavelength under different force in V3 direction.

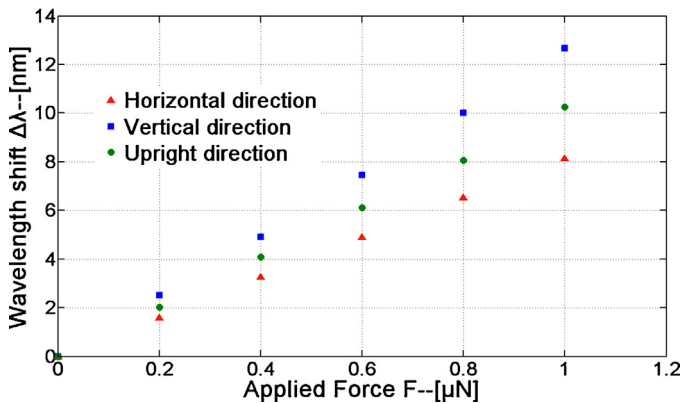


Fig. 10. The relationship between the displacement of resonant wavelength ($\Delta\lambda$) and the applied force (F) in three directions.

5. Conclusion

Through the theoretical analysis and simulation results, the sensor proposed above is demonstrated that it can be used to detect nanomechanical force in the three dimensional space. Robust sensing properties are achieved by designing and optimizing a novel structure which consists of a shoulder-coupled aslant resonant nanocavity and a single pillar. High sensitivity of 8.2, 12.5 and 10.9 nm/ μ N in the horizontal, vertical direction and upright direction are obtained, respectively. And small detectable limit of 24, 16 and 18 nN in the horizontal, vertical direction and upright direction are obtained, respectively. This structure can be used in the three dimensional environment that nanomechanical force needed to detected accurately. Furthermore, this 3D nanomechanical sensor can be integrated to form a nanomechanical sensor array which is hopeful in the future sensing area.

Acknowledgements

This research was supported by NSFC (No. 61372038), National 973 Program (No. 2012CB315705) and Fund of State Key Laboratory of Information Photonics and Optical Communications (Beijing University of Posts and Telecommunications), P.R. China.

References

[1] C. Zhong, C. Shen, Y. You, J. Chu, X. Zou, X. Dong, Y. Jin, J. Wang, Temperature-insensitive optical fiber two-dimensional micrometric displacement sensor based on an in-line Mach-Zehnder interferometer, *J. Opt. Soc. Am. B* 29 (5) (2012) 1136–1140.

[2] B. Dong, J. Hao, C. Liaw, B. Lin, S.C. Tjin, Simultaneous strain and temperature measurement using a compact photonic crystal fiber inter-modal interferometer and a fiber Bragg grating, *Appl. Opt.* 49 (32) (2010) 6232–6235.

[3] Y. Wang, C.R. Liao, D.N. Wang, Embedded coupler based on selectively infiltrated photonic crystal fiber for strain measurement, *Opt. Lett.* 37 (22) (2012) 4747–4749.

[4] A.K. Naik, M.S. Hanay, W.K. Hiebert, X.L. Feng, M.L. Roukes, Towards single-molecule nanomechanical mass spectrometry, *Nature Nanotechnol.* 4 (2009) 445–450.

[5] C. Hierold, A. Jungen, C. Stampefer, T. Helbling, Nano electromechanical sensors based on carbon nanotubes, *Sens. Actuators A Phys.* 136 (1) (2007) 51–61.

[6] E. Yablonovitch, Inhibited spontaneous emission in solid-state physics and electronics, *Phys. Rev. Lett.* 58 (20) (1987) 2059–2062.

[7] S. John, Strong localization of photons in certain disordered dielectric superlattices, *Phys. Rev. Lett.* 58 (23) (1987) 2486–2489.

[8] S. Kita, S. Hachuda, S. Otsuka, T. Endo, Y. Imai, Y. Nishijima, H. Misawa, T. Baba, Super-sensitivity in label-free protein sensing using a nanoslot nanolaser, *Opt. Express* 19 (18) (2011) 17683–17690.

[9] S. Pal, E. Guillelmain, R. Sriram, B.L. Miller, P.M. Fauchet, Silicon photonic crystal nanocavity-coupled waveguides for error-corrected optical biosensing, *Biosensors Bioelectron.* 26 (10) (2011) 4024–4031.

[10] W. Lai, S. Chakravarty, Y. Zou, R.T. Chen, Silicon nano-membrane based photonic crystal microcavities for high sensitivity bio-sensing, *Opt. Lett.* 37 (7) (2012) 1208–1210.

[11] W.-C. Lai, S. Chakravarty, X. Wang, C. Lin, R.T. Chen, On-chip methane sensing by near-IR absorption signatures in a photonic crystal slot waveguide, *Opt. Lett.* 36 (6) (2011) 984–986.

[12] A.E. Serebryannikov, A. Lakhtakia, Optical characteristics of a two-dimensional dielectric photonic crystal immersed in a coherent atomic gas, *J. Opt. Soc. Am. B* 29 (3) (2012) 328–334.

[13] M.T. Tinker, J.-B. Lee, Thermo-optic photonic crystal light modulator, *Appl. Phys. Lett.* 86 (22) (2005) 1797–1803.

[14] C. Lee, J. Thillaigovindan, Optical nanomechanical sensor using a silicon photonic crystal cantilever embedded with a nanocavity resonator, *Appl. Opt.* 48 (10) (2009) 1797–1803.

[15] D. Yang, H. Tian, N. Wu, Y. Yang, Y. Ji, Nanoscale torsion-free photonic crystal pressure sensor with ultra-high sensitivity based on side-coupled piston-type microcavity, *Sens. Actuators A Phys.* 199 (2013) 30–36.

[16] B. Li, C. Lee, NEMS diaphragm sensors integrated with triple-nano-ring resonator, *Sens. Actuators A Phys.* 172 (2011) 61–68.

[17] F. Tian, G. Zhou, Y. Du, F.S. Chau, J. Deng, R. Akkipeddi, Out-of-plane nanomechanical tuning of double-coupled one-dimensional photonic crystal cavities, *Opt. Lett.* 38 (12) (2013) 2005–2007.

[18] M. Winger, T.D. Blasius, T.P.M. Alegre, A.H. Safavi-Naeini, S. Meenehan, J. Cohen, S. Stobbe, O. Painter, A chip-scale integrated cavity-electro-optomechanics platform, *Opt. Express* 19 (25) (2011) 24905–24921.

[19] Y. Yang, D. Yang, H. Tian, N. Wu, Y. Ji, Photonic crystal stress sensor with high sensitivity in double directions based on shoulder-coupled aslant nanocavity, *Sens. Actuators A Phys.* 193 (2013) 149–154.

[20] Z. Xu, L. Cao, C. Gu, Q. He, G. Jin, Micro displacement sensor based on line-defect resonant cavity in photonic crystal, *Opt. Express* 14 (1) (2006) 298–305.

[21] C. Lee, R. Radhakrishnan, C.C. Chen, J. Li, J. Thillaigovindan, N. Balasubramanian, Design and modeling of a nanomechanical sensor using silicon photonic crystals, *J. Lightw. Technol.* 26 (27) (2008) 839–846.

[22] L. Fan, L.T. Varghese, Y. Xuan, J. Wang, B. Niu, M. Qi, Direct fabrication of silicon photonic devices on a flexible platform and its application for strain sensing, *Opt. Express* 20 (18) (2012) 20564–20575.

[23] X. Zhao, J.M. Tsai, H. Cai, X.M. Ji, J. Zhou, M.H. Bao, Y.P. Huang, D.L. Kwong, A.Q. Liu, A nano-opto-mechanical pressure sensor via ring resonator, *Opt. Express* 20 (8) (2012) 8535–8542.

[24] <http://ab-initio.mit.edu/wiki/index.php/Meep>.

[25] E. Eleftheriou, T. Antonakopoulos, G.K. Binnig, G. Cherubini, M. Despont, A. Dhoklaka, U. Dürig, M.A. Lantz, H. Pozidis, H.E. Rothuizen, P. Vettiger, Millipede-a MEMS-based scanning-probe data-storage system, *IEEE Trans. Magn.* 39 (2) (2003) 938–945.

[26] P. Vettiger, G. Cross, M. Despont, U. Drechsler, U. Dürig, B. Gottmann, W. Häberle, M.A. Lantz, H.E. Rothuizen, R. Stutz, G.K. Binnig, The millipede-nanotechnology entering data storage, *IEEE Trans. Nanotechnol.* 1 (1) (2002) 39–55.

Biographies

Yi Yang received the bachelor's degree of Electronic Information Engineering from Beijing University of Posts and Telecommunications (BUPT) in 2011. He is currently a master candidate in the State Key Laboratory of Information Photonics and Optical Communications, Beijing University of Posts and Telecommunications (BUPT), Beijing, P.R. China. His research now focuses on the area of photonic crystals and sensors.

Huiping Tian received the BS and PhD degrees from Shanxi University, Shanxi, China, in 1998 and 2003, respectively. Now she is a professor in the School of Information and Communication Engineering, Beijing University of Posts and Telecommunications (BUPT), Beijing, China. Her research interests are focused on

the area of ultra-short and ultra-fast process in the transmission of optics, photonic crystals and broadband information networking.

Daquan Yang received the bachelor's degree of Electronic Information Science and Technology from JiNan University in 2009. He is currently a PhD candidate in the State Key Laboratory of Information Photonics and Optical Communications, Beijing University of Posts and Telecommunications (BUPT), Beijing, P.R. China. His research now focuses on the area of photonic crystals and optical communication.

Nannan Wu received the bachelor's degree of Communication Engineering from Shandong Normal University in 2011. He is currently a master candidate in the State Key Laboratory of Information Photonics and Optical Communications, Beijing University of Posts and Telecommunications (BUPT), Beijing, P.R. China. His research now focuses on the area of infrared ray absorption.

Jian Zhou received the bachelor's degree of Electronic Information Science and Technology from Nanjing University of Posts and Telecommunications (NUPT) in

2012. He is currently a master candidate in the State Key Laboratory of Information Photonics and Optical Communications, Beijing University of Posts and Telecommunications (BUPT), Beijing, PR China. His research now focuses on the area of photonic crystals and sensors.

Qi Liu received the bachelor's degree of Telecommunication Engineering from Shandong University in 2012. She is currently a master candidate in the State Key Laboratory of Information Photonics and Optical Communications, Beijing University of Posts and Telecommunications (BUPT), Beijing, P.R. China. Her research now focuses on the area of photonic crystals and sensors.

Yuefeng Ji received the PhD degree from Beijing University of Posts and Telecommunications (BUPT), Beijing, China. Now he is a professor in BUPT. His research interests are primarily in the area of broadband communication networks and optical communications, with emphasis on key theory, realization of technology and applications.